GEOLOGICA CARPATHICA, DECEMBER 2019, 70, 6, 471–482 doi: 10.2478/geoca-2019-0027

Decompressional equilibration of the Midsund granulite from Otrøy, Western Gneiss Region, Norway

JOHANNA HOLMBERG[1], MICHAŁ BUKAŁA[2], PAULINE JEANNERET[1], IWONA KLONOWSKA[1,2] and JAROSŁAW MAJKA[1,2,✉]

[1]Department of Earth Sciences, Uppsala University, Villavägen 16, 752 36 Uppsala, Sweden; ✉ jaroslaw.majka@geo.uu.se
[2]Faculty of Geology, Geophysics and Environmental Protection, AGH University of Science and Technology, Mickiewicza 30, 30-059 Kraków, Poland

(Manuscript received June 10, 2019; accepted in revised form October 24, 2019)

Abstract: The Western Gneiss Region (WGR) of the Scandinavian Caledonides is an archetypal terrain for high-pressure (HP) and ultrahigh-pressure (UHP) metamorphism. However, the vast majority of lithologies occurring there bear no, or only limited, evidence for HP or UHP metamorphism. The studied Midsund HP granulite occurs on the island of Otrøy, a locality known for the occurrence of the UHP eclogites and mantle-derived, garnet-bearing ultramafics. The Midsund granulite consists of plagioclase, garnet, clinopyroxene, relict phengitic mica, biotite, rutile, quartz, amphibole, ilmenite and titanite, among the most prominent phases. Applied thermodynamic modelling in the NCKFMMnASHT system resulted in a pressure–temperature (P–T) pseudosection that provides an intersection of compositional isopleths of X_{Mg} (Mg/Mg+Fe) in garnet, albite in plagioclase and X_{Na} (Na/Na+Ca) in clinopyroxene in the stability field of melt+plagioclase+garnet+clinopyroxene+amphibole+ilmenite. The obtained thermodynamic model yields P–T conditions of 1.32–1.45 GPa and 875–970 °C. The relatively high P–T recorded by the Midsund granulite may be explained as an effect of equilibration due to exhumation from HP (presumably UHP) conditions followed by a period of stagnation under HT at lower-to-medium crustal level. The latter seems to be a more widespread phenomenon in the WGR than previously thought and may well explain commonly calculated pressure contrasts between neighboring lithologies in the WGR and other HP–UHP terranes worldwide.

Keywords: Scandinavian Caledonides, thermodynamic modelling, granulite facies metamorphism, decompression.

Introduction

A multitude of recent studies have shown that continental crust can be subducted to mantle depths during collisional orogenies (see Gilotti 2013 and references therein). This process results in densification of the subducting continental plate due to formation of mineral assemblages that are stable under high- to ultrahigh-pressure (HP–UHP) conditions. Hence, both mafic and felsic protoliths that are present in the subducting plate should be transformed into eclogites and HP–UHP gneisses that contain index minerals typical for eclogite facies conditions. However, it is known from both field observations and through petrological studies (e.g., Young & Kylander-Clark 2015) that the majority of the rock volume in HP–UHP terranes shows little to no evidence for metamorphism under eclogite facies conditions. This phenomenon generally results from either overstepping of metamorphic reactions (e.g., Castro & Spear 2017) or from pervasive re-equilibration of eclogitic assemblages during exhumation (e.g., Engvik et al. 2018). A combination of both is also possible. Thus, the commonly observed plagioclase-bearing mineral assemblages could either have been effectively metastable during the peak metamorphism, because the kinetic barrier for the formation of jadeite +quartz at the expense of plagioclase has not been overcome, or have been formed during retrogression. In turn, there may be various reasons for the aforementioned phenomena. The most prominent reasons include the variability in the subduction and exhumation rates, availability of fluids, and the rock bulk chemistry (e.g., Hacker et al. 2003).

Here, we report results from a granulite that was sampled on the island of Otrøy in the Western Gneiss Region (WGR), Scandinavian Caledonides, which is a well-known locality for exposures of UHP eclogites and ultramafic rocks (e.g., Kylander-Clark et al. 2007; van Roermund 2009a,b). We demonstrate through petrography, coupled with phase equilibrium thermodynamic modelling, that the bulk chemical composition of the examined granulite allowed for the stabilization of the plagioclase-bearing assemblage under relatively high pressure. We suggest that the observed mineral assemblage is an effect of decompressional equilibration during exhumation from HP (presumably even UHP) conditions, associated with limited partial melting. Notwithstanding the above considerations, the studied Midsund granulite provides additional evidence for a complex subduction–exhumation history recorded by continental crust of the WGR in the Scandinavian Caledonides.

Geological setting

The Scandinavian Caledonides (Fig. 1A) formed as a result of Ordovician closure of the Iapetus Ocean and subsequent

collision of Laurentia and Baltica in the late Silurian/early Devonian (Gee 1975; Corfu et al. 2006, 2014; Gee et al. 2008, 2013). This continent–continent collisional event caused: (1) the amalgamation and thrusting of oceanic and continental allochthons (the Lower, Middle, Upper and Uppermost allochthons) towards the east-southeastward over the autochthonous basement (Roberts & Gee 1985; Roberts 2003); and (2) during the final stages of orogenesis, the westward continental subduction of part of the Baltica basement with segments of overlying allochthons beneath Laurentia that resulted in HP–UHP metamorphism (e.g., Gee 1975; Andersen et al. 1991, 1998; Kylander-Clark et al. 2007, 2008; Walsh et al. 2007; Gee et al. 2013; DesOrmeau et al. 2015; Gordon et al. 2016). In many areas, thrust imbrication and later extensional deformation,

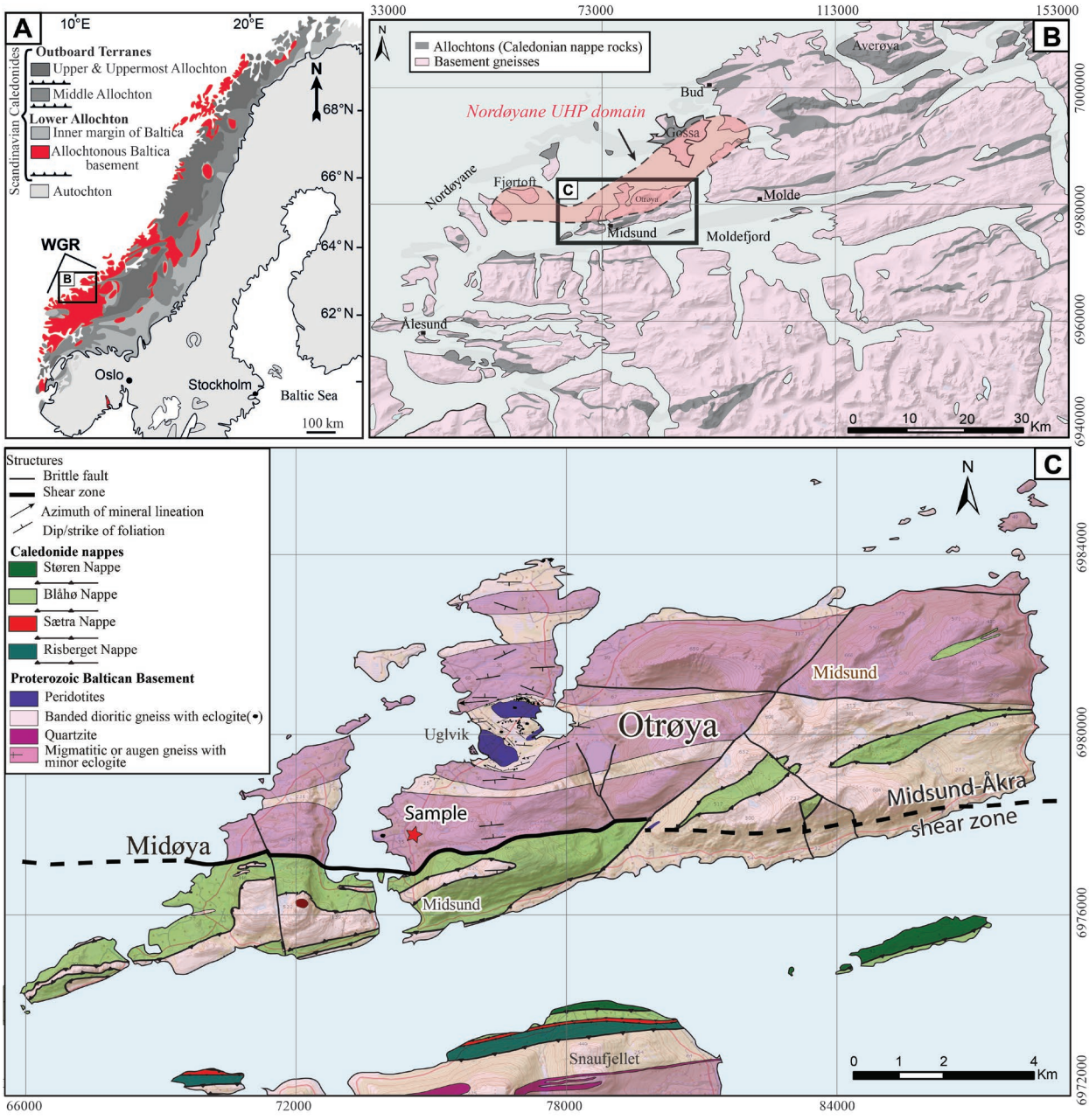

Fig. 1. A — Simplified tectonostratigraphic map of the Scandinavian Caledonides with inferred provenance of the major tectonic units (modified after Gee et al. 2010). In red the Allochthonous Baltica basement including the Western Gneiss Region (WGR) is marked. **B** — Simplified geological map of the Molde–Ålesund region belonging to the WGR that consists of allochthonous Caledonide nappes (in dark grey) infolded into Baltica basement gneisses (in pink). The study area is outlined by the black rectangle and shown in more detail in Fig. 1C. **C** — Geological map of Otrøy Island showing occurrences of peridotites and eclogites within the Proterozoic basement gneisses in the northern part; separated from the southern allochthonous sequence, the Blåhø Nappe (modified after van Roermund et al. 2005; Carswell et al. 2006; Spengler 2006; Hollocher et al. 2007; van Roermund 2009a; Hacker et al. 2010). The locations of sample documented and discussed in this paper is outlined by the red star (EUREF89 NTM 74550 m E, 6977750 m N).

including folding, resulted in the juxtaposition and tight interfolding of the nappes and basement rocks, particularly along the western coast of Norway (Fig. 1A,B; Gee 1980; Krill 1980; Tucker 1986; Robinson 1995; Braathen et al. 2000; Robinson & Hollocher 2008; Gee et al. 2010). Throughout the Scandinavian Caledonides, the occurrence of numerous windows in the allochthonous nappes exposes the parautochthonous Baltica basement rocks (Fig. 1A; Roberts & Gee 1985; Roberts 2003). The WGR, representing the hinterland of the Scandinavian Caledonides, is one of those tectonic windows and corresponds to the deepest exposed structural level (Gee 1975) and the largest exposure of parautochtonous basement (Fig. 1B). The basement of the WGR consists mainly of granitic, granodioritic, and tonalitic gneisses of Proterozoic age (Fig. 1B) that were formed c. 1690–1620 Ma (Brueckner 1972; Carswell & Harvey 1985; Harvey 1985; Tucker et al. 1990; Skår 2000; Austrheim et al. 2003; Corfu et al. 2014; DesOrmeau et al. 2015; Young 2017). The basement rocks were subsequently: (1) overprinted by granulite-facies metamorphism related to the Sveconorwegian orogeny at c. 1100–900 Ma that was associated with pluton and dyke emplacement and local migmatization (Skår & Pedersen 2003; Røhr et al. 2004, 2013; Tucker et al. 2004; Root et al. 2005; Glodny et al. 2008; Kylander-Clark et al. 2008; Krogh et al. 2011; Corfu et al. 2014; DesOrmeau et al. 2015); and (2) reworked during the Caledonian orogeny (e.g., Fossen 2010). High-grade metamorphism, reaching HP–UHP conditions, occurred during the final stages of the Scandian collision at c. 420 to 400 Ma (e.g., Kylander-Clark et al. 2008; Hacker et al. 2010; Krogh et al. 2011). This was followed by a lower-pressure (1.5–0.5 GPa), granulite/amphibolite facies overprint at 400–385 Ma (Terry et al. 2000; Kylander-Clark et al. 2007, 2008; Walsh et al. 2007; Krogh et al. 2011; DesOrmeau et al. 2015; Hacker et al. 2015; Holder et al. 2015).

The UHP rocks (eclogites and quartzofeldspathic gneisses) crop out at three discrete areas within the WGR. These are the southern (Nordfjord), central (Sørøyane), and northern (Nordøyane) UHP domains (e.g., Hacker et al. 2010; Butler et al. 2013; Smith & Godard 2013; DesOrmeau et al. 2015). Overall, these UHP rocks show a northeasterly increase in the peak UHP metamorphic conditions from 750 °C and 3.5 GPa in the Nordfjord UHP domain (e.g., Cuthbert et al. 2000; Young et al. 2007; Smith & Godard 2013; DesOrmeau et al. 2015; Butler et al. 2018) to 820–850 °C and 3.8–3.9 GPa in the Nordøyane UHP domain (Fig. 1B; e.g., Terry et al. 2000; Carswell et al. 2006; DesOrmeau et al. 2015). Even higher P–T estimates (850–950 °C and 5.5–6.5 GPa) have been suggested for orthopyroxene eclogites and garnet websterites hosted by gneisses of the northern WGR in the Moldefjord region (including Otrøy island of the Nordøyane UHP domain; Fig. 1B; Vrijmoed et al. 2006, 2008; Scambelluri et al. 2008; Spengler et al. 2009; van Roermund 2009a,b). The Nordøyane UHP domain extends from the islands of Nordøyane to the nearby mainland, and includes the northernmost UHP rocks exposed in the WGR (Butler et al. 2013).

The sample discussed in this paper was obtained from the Proterozoic Baltica basement exposed on Otrøy in the northwestern part of the WGR in the Nordøyane UHP domain (Fig. 1B,C). A simplified geologic map of the island is shown in Figure 1C. Otrøy is characterized by E–W to NNE–SSW trending belts of basement rocks. These belts consist of interlayered migmatitic or augen orthogneisses and well layered dioritic-gneisses (resembling the so-called Ulla Gneiss *sensu* Terry & Robinson 2004) with abundant lenses of eclogites that preserve eclogite facies mineral assemblages to various extents (Carswell et al. 2006), garnet peridotites, and minor eclogitized gabbros (van Roermund 2009b). The dominant ENE–WSW striking amphibolite facies foliation is subvertical, commonly associated with a well-developed subhorizontal E–W amphibolite-facies lineation (Spengler 2006). In the northwestern part of the island, three occurrences of Caledonized UHP Mg–Cr garnet-peridotite bodies are incorporated within the basement gneisses (van Roermund & Drury 1998; Brueckner et al. 2002; Carswell et al. 2006; van Roermund 2009b).

The southern part of the island is separated from the northern part by the Midsund–Åkra shear zone (Fig. 1C). This major shear zone is a greenschist-facies ductile shear zone with a dominant strike-slip sense of displacement associated with a well-developed subhorizontal lineation (Terry & Robinson 2004). The rocks belonging to the southern part form an assemblage of metasediments (Blåhø Nappe mica schists), metabasites and orthogneisses. An extensive part of the basement along the southern shores consist of homogeneous amphibolite boudins and finely laminated, pinkish feldspathic gneiss with deformed diabase dykes (Hollocher et al. 2007).

Analytical procedures

The mineral chemistry data presented below was determined using a JXA8530F Jeol Hyperprobe Field Emission Electron Probe Microanalyser (FE-EPMA) at the Department of Earth Sciences, Uppsala University, Sweden. The measurements were carried out using a 15kV accelerating voltage and a 10nA beam current. The counting times were 10 s for the peaks and 5 s for the background. Both mineral and synthetic oxide standards were used to calibrate the Kα lines for all measured elements. The raw data was corrected according to the PAP routine.

Results

Field observations

The Proterozoic Baltica basement exposed in an abandoned quarry located in Midsund is shown on Figs. 1C & 2A. The rocks exposed in this quarry consist mainly of migmatitic banded dioritic gneiss (Fig. 2B) that are interlayered with granitoidic augen-orthogneiss (Fig. 2C). These gneisses are

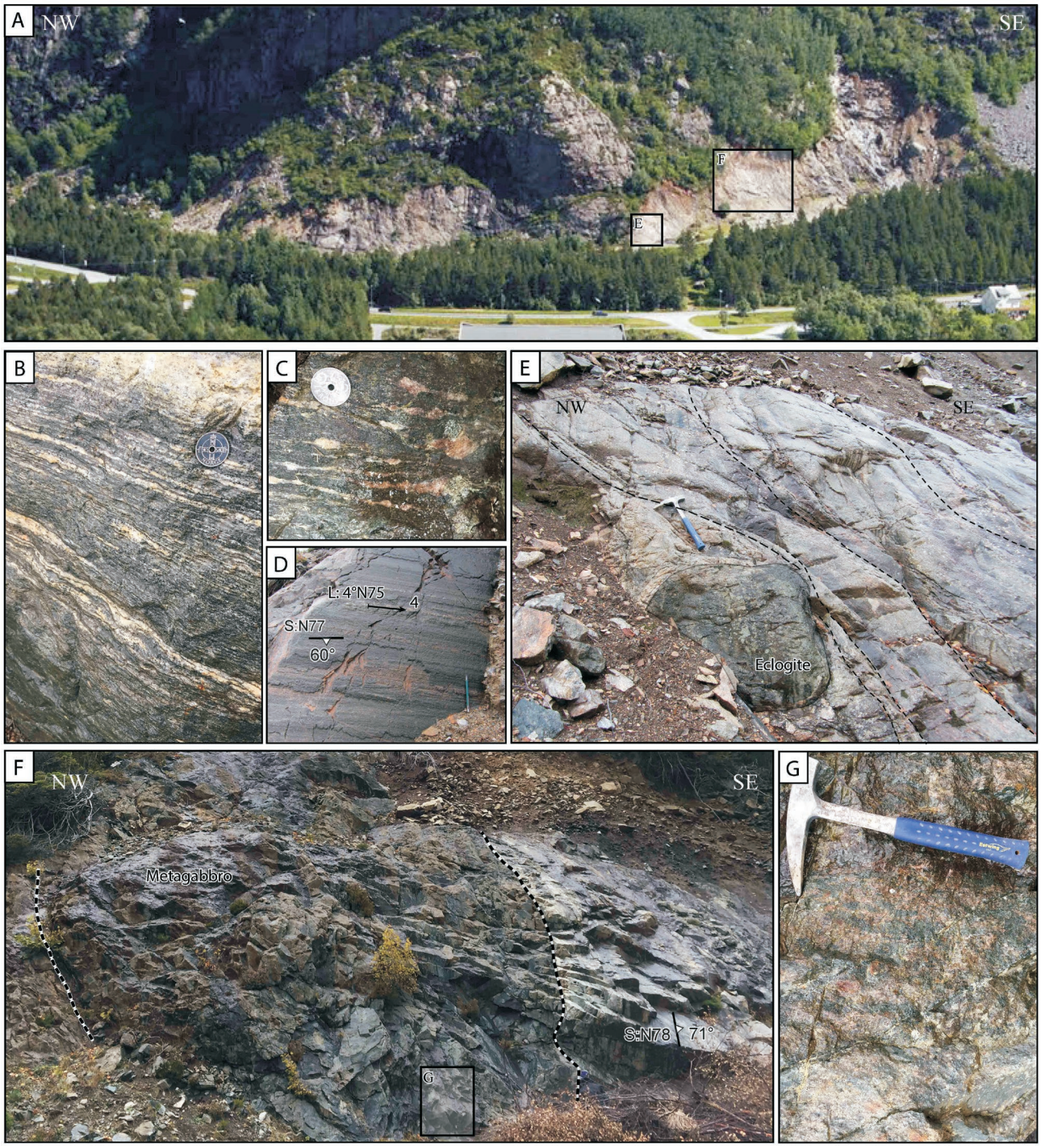

Fig. 2. Outcrop photos from a former quarry located in the western part of Otrøy Island, where the sample discussed in this paper is located, showing the lithological and structural features of Proterozoic basement rocks of Baltica. **A** — Panoramic view of the entire outcrop from the SW (from Google maps). **B, C** — Proterozoic basement consisting of (B) migmatitic banded dioritic gneiss interlayered with (C) Kfs-augen-orthogneiss. **D** — Penetrative steeply dipping foliation striking ~ENE–WSW within augen-orthogneiss, with penetrative mineral lineation defined by elongated K-feldspar and quartz. Lineation has subhorizontal plunge and ENE–WSW azimuth. **E** — Lens of eclogite and retro-eclogite within the strongly foliated augen-orthogneiss. **F** — HP granulite embedded within the migmatitic banded dioritic gneiss. **G** — Zoom in on a part of (F): HP granulite with the layered garnet showing the sample discussed in this paper.

affected by a penetrative, steeply dipping amphibolite-facies foliation that strikes ~ENE–WSW. A linear shape fabric is well defined by elongate grain aggregates of either K-fedspar or quartz (commonly ribbons) and has a subhorizontal plunge and ENE–WSW azimuth (Fig. 2D). Eclogites, retro-eclogites and granulites occur as isolated lenses and boudins within

both the foliated augen-orthogneiss (Fig. 2E) and the migmatitic banded dioritic gneiss (Fig. 2F,G).

Petrography and mineral chemistry

The Midsund granulite exhibits a grano- to nematoblastic texture and is dominated by garnet, clinopyroxene, plagioclase and quartz (Fig. 3A,B). A weak foliation is marked by less abundant amphibole and biotite, minor apatite, rutile, and titanite that occur sporadically in the matrix (Fig. 3A,B). Even less abundant are phengite, ilmenite, zircon and K-feldspar.

Garnet forms subhedral to anhedral porphyroblasts and is generally homogeneous in its composition in the range of $Alm_{47–49}Grs_{31–35}Prp_{17–18}Sps_{0.8–1.5}$ (Table 1, Fig. 3C). The only exception in this pattern is the thin outermost rim that shows a sharp increase of X_{Alm} (up to 56 mol. %) and X_{Fe} (from 72 to 75 %) that is accompanied by a simultaneous decrease of X_{Grs} (down to 23 mol. %), while X_{Prp} and X_{Sps} remain relatively consistent across the whole profile (Fig. 3C,D). Garnet contains scarce inclusions of sodic clinopyroxene, phengite, quartz, apatite, rutile, ilmenite and zircon, which presumably represents a mineral assemblage entrapped during the prograde to peak metamorphism. Seldom composite inclusions of phengite partly replaced by biotite, and inclusions of amphibole and plagioclase were found in fissured garnet grains, indicating their retrograde origin. Rarely, multi-phase inclusions, somewhat resembling melts (see e.g., Ferrero et al. 2015), composed of K-feldspar, biotite, plagioclase and/or pure albite are also found in the garnet (Fig. 3E).

Clinopyroxene of diopside composition rarely occurs as elongated inclusions (not exceeding 200 μm) in garnet (Table 1, Fig. 3D). Most commonly, clinopyroxene forms poikilitic intergrowths with plagioclase, quartz and amphibole in the matrix (Fig. 3B,F), and its composition shows a broad range, i.e. X_{Di}=79–93 mol. %, X_{Jd}=6–18 mol. % (X_{Na}=0.07–0.21) and X_{Aeg}=1–4 mol. % (Table 1). Matrix clinopyroxene is generally well preserved and is only locally replaced by amphibole (Fig. 3F).

Phengite has only been found as inclusions in garnet and partially replaced by biotite (Fig. 3G). The Si content varies between 3.17 and 3.20 a.p.f.u. (Table 2).

Plagioclase occurs in four textural positions. Most commonly, it forms subhedral grains (up to 600 μm) evenly distributed in the matrix (Fig. 3H), hereinafter referred to as matrix plagioclase. It is a Na-rich variety with X_{Ab}=75–78 mol. %, X_{An}=17–22 mol. % and X_{Or}=3–5 mol. % (Table 3). Plagioclase is also a major constituent of poikilitic intergrowths with clinopyroxene (Fig. 3B,F). The chemical composition of this plagioclase corresponds to X_{Ab}=75–77 mol. %, X_{An}=19–21 mol. % and X_{Or}=2–4 mol. % (Table 3). Sporadically, plagioclase also forms intergrowths with biotite and monomineral inclusions in garnet.

Amphibole predominantly forms euhedral to subhedral, uniformly oriented elongated grains in the matrix. They contain abundant quartz and apatite inclusions, and is rarely observed to have partly replaced poikiloblastic clinopyroxene (Fig. 3F), but it also forms intergrowth with quartz. In both textural positions, amphibole has a pargasitic composition (Table 2).

Biotite mainly forms subhedral flakes (with sizes varying from 50 μm to 1.5 mm) located in the matrix. Less common larger flakes (>500 μm) are typically oriented (sub-)parallel to amphibole (Fig. 3B). However, the orientation of some grains is at a high-angle to the amphiboles. Biotite is also found as inclusions partly replacing phengite in garnet (Fig. 3G).

Quartz is an abundant mineral that is evenly distributed in the matrix (Fig. 3A,B). Quartz grains often display polygonal textures with straightened grain boundaries (e.g., Humphreys & Hatherley 1995) and distinctive triple junctions at the grain boundaries (e.g., Kruhl 2001). These preserved textures are indicative of the high-temperature GBAR (grain boundary area reduction) process.

In summary, based on the above-mentioned petrographic description, it is inferred that the studied rock underwent HP metamorphism, which was followed by a lower pressure granulite facies overprint. The latter resulted in the stabilization of the peak temperature assemblage composed of garnet+plagioclase+clinopyroxene+ilmenite±amphibole ±melt.

Pressure–temperature estimates

Isochemical phase diagrams have been calculated using the Perple_X 6.8.5 software package (Connolly 1990, 2005). The internally consistent thermodynamic database by Holland & Powell (2011) has been used for calculations in the Na_2O–CaO–K_2O–FeO–MgO–MnO–Al_2O_3–SiO_2–H_2O–TiO_2 (NCKFMMnASHT) system. The granulite chemical composition was determined by areal-EDS analyses performed in the same electron microprobe laboratory as the WDS measurements. Results are presented in Figure 4. To estimate the minimum fluid content required to produce melt within the granulite-facies assemblage observed in the thin section, the P–X_{H2O} pseudosection was modelled. A pure H_2O fluid was assumed for the modelling. The pseudosection was calculated in a P–T space of 1–2 GPa and 650–1100 °C and a constant H_2O content of 0.40 wt. % (Fig. 4). Solution models for garnet, biotite and ilmenite are from White et al. (2007), white mica and melt from White et al. (2014), clinopyroxene from Green et al. (2007), plagioclase from the ternary feldspar model of Holland & Powell (2003), and amphibole from Green et al. (2016) have been selected.

Compositional isopleths of X_{Mg} (X_{Mg}=Mg/Mg+Fe) in garnet, albite content in plagioclase and X_{Na} (X_{Na}=Na/Na+Ca) in clinopyroxene have been combined to estimate P–T conditions of equilibration. Isopleths intersect within the field containing the phase assemblage of melt+plagioclase+garnet+clinopyroxene+amphibole+ilmenite (Fig. 4). The P–T space encompassed by the intersection of the isopleths shows that the granulite assemblage observed in the studied sample has formed at HP and HT conditions of 1.32–1.45 GPa and 875–970 °C.

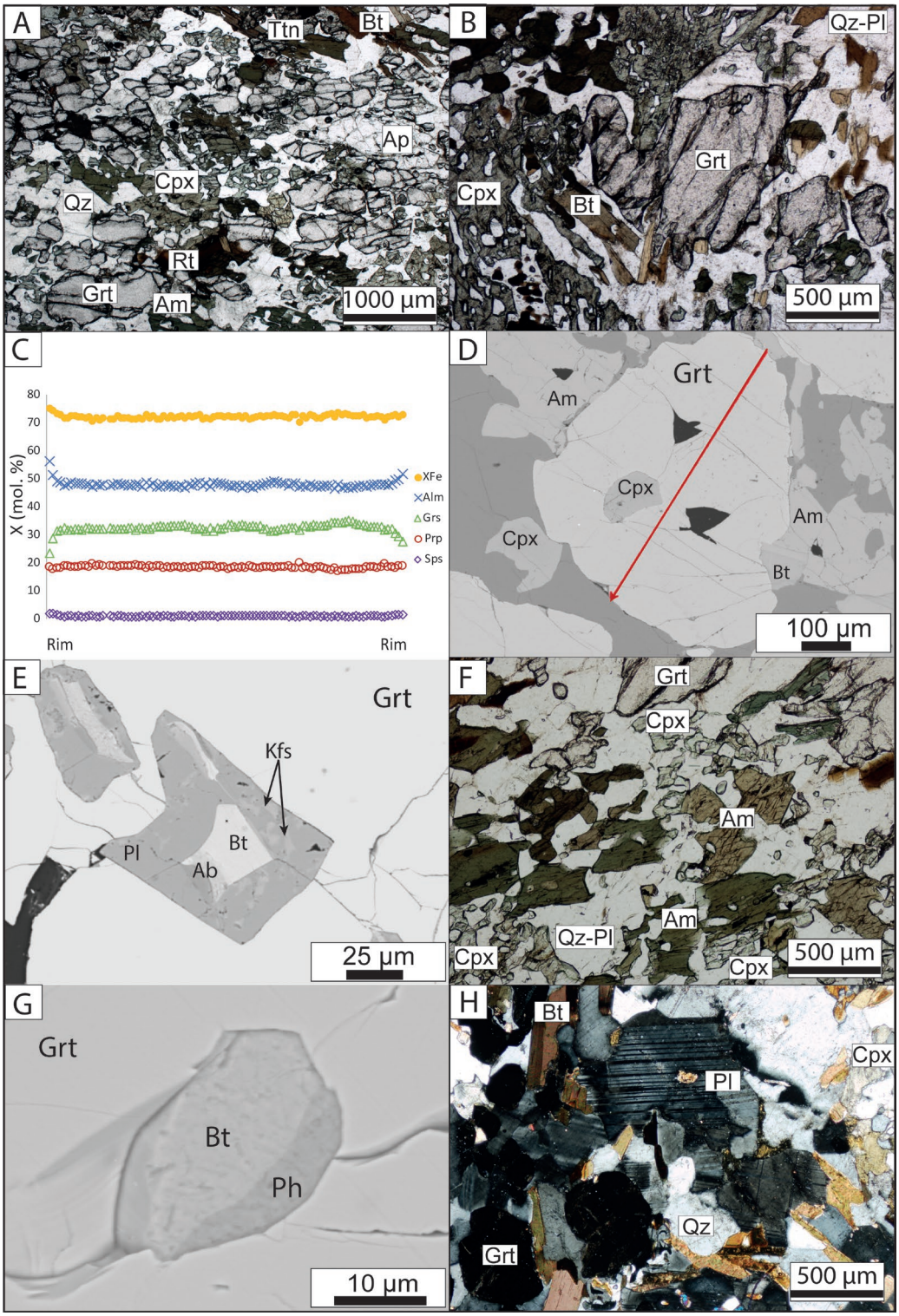

Fig. 3. A, B — Photomicrographs in a plane polarized light. (A) Typical microtexture and composition of granulite (sample IK14-11-A3) with garnet (Grt), clinopyroxene (Cpx), quartz (Qz), plagioclase (Pl), amphibole (Am), biotite (Bt), minor titanite (Ttn), rutile (Rt) and apatite (Ap). (B) Typical garnet and retrogressed poikiloblastic clinopyroxene with plagioclase and quartz intergrowths. **C** — Compositional profile across the garnet presented in (D) shows variations in mole fractions of the X_{Fe} and almandine (Alm), grossular (Grs), pyrope (Prp) and spessartine (Sps) components. **D** — BSE image of a garnet with a trajectory line marked along which a step line profile was carried out. Garnet shows an inclusion of clinopyroxene and it is surrounded by amphibole, biotite and clinopyroxene. **E** — BSE image of a multiphase inclusion of biotite+plagioclase+K-feldspar (Kfs)+albite (Ab) in garnet. **F** — Photomicrograph in a plane polarized light showing amphibole replacing poikiloblastic clinopyroxene. **G** — BSE image of a composite inclusion of phengite (Ph) and biotite in garnet. **H** — Photomicrograph in a crossed polarized light showing plagioclase with polysynthetic twinning evenly distributed in the matrix together with biotite, quartz, clinopyroxene and garnet.

Table 1: Representative microprobe analyses of garnet and clinopyroxene.

Mineral	Grt	Grt	Grt	Grt	Grt	Grt	Grt	Grt	Grt	Grt	Cpx	Cpx	Cpx	Cpx	Cpx	Cpx	Cpx	Cpx	Cpx	Cpx
Position	Rim	Rim	Rim	Core	Core	Core	Core	Rim	Rim	Rim	Pbl	Pbl	Pbl	Pbl	Pbl	Pbl	Incl	Incl	Incl	Incl
SiO_2	37.72	38.10	38.30	38.13	38.34	37.86	37.76	37.61	37.46	37.77	51.39	51.32	51.13	50.63	50.96	50.69	50.02	49.11	51.13	51.63
TiO_2	0.06	0.02	0.08	0.12	0.02	0.09	0.11	0.06	0.09	0.01	0.22	0.34	0.28	0.33	0.32	0.36	0.35	0.33	0.31	0.31
Al_2O_3	21.61	21.79	21.82	21.85	21.84	22.20	21.76	21.40	21.56	21.50	7.17	3.88	7.60	5.20	7.84	6.63	6.95	6.22	6.10	5.65
CaO	8.55	10.38	11.37	12.14	12.20	12.55	13.01	11.30	10.64	9.99	18.88	21.83	18.71	21.11	19.16	19.74	21.83	22.09	21.95	22.32
MgO	4.82	4.62	4.69	4.85	4.75	4.51	4.58	4.84	4.92	4.94	9.92	11.56	9.71	10.89	10.02	9.63	10.94	10.76	11.19	12.02
MnO	0.93	0.86	0.68	0.48	0.53	0.40	0.39	0.72	0.70	0.73	0.09	0.11	0.12	0.06	0.09	0.14	0.08	0.08	0.00	0.04
FeO	26.21	23.81	22.89	22.41	22.38	22.47	22.10	23.22	22.88	23.87	8.77	9.89	9.23	9.43	9.19	9.99	9.63	9.35	8.15	7.43
Na_2O	0.00	0.06	0.01	0.05	0.05	0.07	0.09	0.04	0.02	0.04	2.84	0.96	2.58	1.37	2.36	1.89	1.01	0.95	1.29	1.26
K_2O	0.00	0.00	0.00	0.00	0.00	0.01	0.00	0.00	0.01	0.00	0.00	0.00	0.00	0.01	0.00	0.00	0.01	0.03	0.00	0.02
Total	99.99	99.81	99.87	100.09	100.16	100.20	99.79	99.22	98.38	98.98	99.37	100.05	99.54	99.11	100.15	99.18	100.96	99.02	100.21	100.89
O	12.00	12.00	12.00	12.00	12.00	12.00	12.00	12.00	12.00	12.00	6.00	6.00	6.00	6.00	6.00	6.00	6.00	6.00	6.00	6.00
Si	2.95	2.97	2.97	2.95	2.96	2.92	2.93	2.94	2.95	2.97	1.90	1.92	1.90	1.90	1.88	1.91	1.85	1.85	1.89	1.89
Ti	0.00	0.00	0.00	0.01	0.00	0.01	0.01	0.00	0.01	0.00	0.01	0.01	0.01	0.01	0.01	0.01	0.01	0.01	0.01	0.01
Al	1.99	2.00	2.00	1.99	1.99	2.02	1.99	1.97	2.00	1.99	0.31	0.17	0.33	0.23	0.34	0.29	0.30	0.28	0.27	0.24
Ca	0.72	0.87	0.95	1.01	1.01	1.04	1.08	0.95	0.90	0.84	0.75	0.87	0.74	0.85	0.76	0.79	0.86	0.89	0.87	0.88
Mg	0.56	0.54	0.54	0.56	0.55	0.52	0.53	0.56	0.58	0.58	0.55	0.64	0.54	0.61	0.55	0.54	0.60	0.60	0.62	0.66
Mn	0.06	0.06	0.04	0.03	0.03	0.03	0.03	0.05	0.05	0.05	0.00	0.00	0.00	0.00	0.00	0.00	0.00	0.00	0.00	0.00
Fe^{2+}	1.71	1.55	1.49	1.45	1.45	1.45	1.43	1.52	1.51	1.57	0.20	0.27	0.25	0.25	0.24	0.30	0.24	0.22	0.23	0.19
Fe^{3+*}											0.07	0.04	0.04	0.05	0.04	0.01	0.05	0.07	0.02	0.04
Na	0.00	0.01	0.00	0.01	0.01	0.01	0.01	0.01	0.00	0.01	0.20	0.07	0.19	0.10	0.17	0.14	0.07	0.07	0.09	0.09
K	0.00	0.00	0.00	0.00	0.00	0.00	0.00	0.00	0.00	0.00	0.00	0.00	0.00	0.00	0.00	0.00	0.00	0.00	0.00	0.00
Total	8.00	8.00	8.00	8.00	8.00	8.00	8.00	8.00	8.00	8.00	4.00	4.00	4.00	4.00	4.00	4.00	4.00	4.00	4.00	4.00
Jad											17.48	5.78	17.55	8.68	15.87	13.79	6.63	5.89	8.91	8.03
Di											78.61	92.79	80.47	89.54	82.10	85.58	92.17	92.51	90.28	90.58
Aeg											3.91	1.43	1.97	1.77	2.04	0.63	1.20	1.60	0.81	1.39
X_{Na}											0.21	0.07	0.20	0.11	0.18	0.15	0.07	0.07	0.09	0.09
X_{Mg}	24.69	25.70	26.75	27.84	27.45	26.35	26.98	27.81	27.71	26.95	73.09	70.69	68.32	71.01	69.68	64.23	71.28	73.30	73.02	77.94
Alm	56.13	51.52	49.22	47.58	47.60	47.82	46.69	49.35	49.75	51.66										
Grs	23.46	28.78	31.33	33.02	33.25	34.22	35.22	30.77	29.64	27.70										
Prp	18.40	17.82	17.98	18.36	18.01	17.11	17.25	18.34	19.07	19.06										
Sps	2.02	1.88	1.47	1.04	1.14	0.86	0.84	1.55	1.55	1.59										

Jad=Al/(Al+Fe^{3+})×(100−Di), Di=(Ca+Fe^{2+}+Mg)/(Ca+Fe^{2+}+Mg)+(2×Na)×100, Aeg=Al/(Al+Fe^{2+})×(100−Di), XNa=Na/(Na+Ca), XMg=Mg/(Fe^{2+}+Mg)×100, Alm=Fe^{2+}/(Fe^{2+}+Mg+Ca+Mn)×100, Grs=Ca/(Ca+Fe^{2+}+Mg+Mn)×100, Prp=Mg/(Mg+Fe^{2+}+Ca+Mn)×100, Sps=Mn/(Mn+Fe^{2+}+Mg+Ca)×100, *Fe^{3+} has been estimated based on charge balance; Pbl — poikiloblast; Inlc — inclusion in garnet

Table 2: Representative microprobe analyses of phengite and amphibole.

Mineral	Ph	Ph	Ph	Ph	Am	Am	Am	Am
Position	Incl	Incl	Incl	Incl	Mtx	Mtx	Mtx	Mtx
SiO_2	48.13	47.63	48.72	49.07	41.01	42.25	40.79	41.56
TiO_2	1.21	1.23	1.00	1.06	1.42	1.78	2.09	1.85
Al_2O_3	30.76	31.18	31.94	31.81	13.82	12.91	13.34	13.37
CaO	0.16	0.14	0.12	0.13	11.47	11.38	11.56	11.44
MgO	3.00	2.54	2.21	2.45	9.81	10.66	10.18	10.25
MnO	0.01	0.00	0.10	0.03	0.03	0.08	0.06	0.03
FeO	2.95	2.43	1.90	2.16	16.10	15.79	15.61	15.59
Na_2O	0.10	0.14	0.14	0.14	1.87	1.93	1.91	1.85
K_2O	10.38	10.74	10.66	10.66	1.59	1.56	1.63	1.50
Total	97.28	96.58	97.19	98.03	97.12	98.34	97.17	97.44
O	11.00	11.00	11.00	11.00	23.00	23.00	23.00	23.00
Si	3.18	3.17	3.20	3.20	6.21	6.28	6.16	6.23
Ti	0.06	0.06	0.05	0.05	0.16	0.20	0.24	0.21
Al	2.40	2.45	2.47	2.45	2.47	2.26	2.38	2.36
Ca	0.01	0.01	0.01	0.01	1.86	1.81	1.87	1.84
Mg	0.30	0.25	0.22	0.24	2.22	2.36	2.29	2.29
Mn	0.00	0.00	0.01	0.00	0.00	0.01	0.01	0.00
Fe^{2+}	0.16	0.14	0.10	0.12	2.04	1.82	1.88	1.84
Fe^{3+*}					0.00	0.14	0.10	0.11
Na	0.01	0.02	0.02	0.02	0.55	0.56	0.56	0.54
K	0.88	0.91	0.89	0.89	0.31	0.30	0.31	0.29
Total	7.00	7.01	6.97	6.98	15.82	15.74	15.80	15.72

*Fe^{3+} has been estimated based on charge balance; Mtx — matrix; Inlc — inclusion in garnet

Table 3: Representative microprobe analyses of plagioclase.

Mineral	Pl	Pl	Pl	Pl	Pl	Pl	Pl	Pl	Pl	Pl
Position	Mtx	Mtx	Mtx	Mtx	Mtx	Mtx	Pbl	Pbl	Pbl	Pbl
SiO_2	63.94	63.65	62.95	62.64	62.20	62.99	62.83	62.36	63.16	62.51
Al_2O_3	21.67	21.91	22.03	22.04	22.56	21.94	22.60	23.01	22.08	22.59
CaO	3.42	3.70	3.89	3.86	4.49	3.97	4.42	4.68	3.90	4.46
Na_2O	8.66	9.01	9.08	8.90	8.57	9.15	8.56	8.73	8.77	8.69
K_2O	0.87	0.72	0.69	0.64	0.56	0.58	0.59	0.40	0.64	0.54
Total	98.56	98.99	98.64	98.08	98.38	98.63	99.00	99.18	98.55	98.79
O	8.00	8.00	8.00	8.00	8.00	8.00	8.00	8.00	8.00	8.00
Si	2.86	2.84	2.83	2.82	2.80	2.83	2.81	2.78	2.83	2.80
Al	1.14	1.15	1.17	1.17	1.20	1.16	1.19	1.21	1.17	1.19
Ca	0.16	0.18	0.19	0.19	0.22	0.19	0.21	0.22	0.19	0.21
Na	0.75	0.78	0.79	0.78	0.75	0.80	0.74	0.76	0.76	0.76
K	0.05	0.04	0.04	0.04	0.03	0.03	0.03	0.02	0.04	0.03
Total	4.97	4.99	5.01	5.00	4.99	5.01	4.98	5.00	4.98	4.99
XAn (Ca)	16.99	17.73	18.40	18.63	21.73	18.71	21.44	22.33	19.00	21.41
XAb (Na)	77.86	78.14	77.72	77.72	75.04	78.02	75.14	75.38	77.30	75.50
XOr (K)	5.15	4.13	3.89	3.66	3.23	3.27	3.42	2.29	3.71	3.09

Mtx — matrix; Pbl — forming poikilitic intergrowths with clinopyroxene

Discussion and final remarks

Garnet grains commonly record valuable information regarding the evolution of a rock. Even though the garnet in the Midsund granulite is nearly completely homogenized and is inclusion-poor, it still provides insight into the prograde to peak-pressure metamorphic evolution of the rock. Rare inclusions of sodic clinopyroxene and phengitic mica are interpreted to have formed during the prograde to near peak-pressure stages of the P–T path. The peak-pressure conditions were impossible to estimate for the studied rock due to severe post-peak pressure processes that lead to the obliteration of the peak assemblage. However, it can be speculated that they were not significantly different from the P–T conditions for Scandian re-equilibration that was calculated for the nearby Ugelvik garnet websterite (c. 3–4 GPa at 800–900 °C, their M3 assemblage, Spengler et al. 2009) or the peak P–T conditions estimated for an UHP eclogite (c. 3–4 GPa at 750–850 °C, Kylander-Clark et al. 2007) located in close proximity to the Midsund granulite.

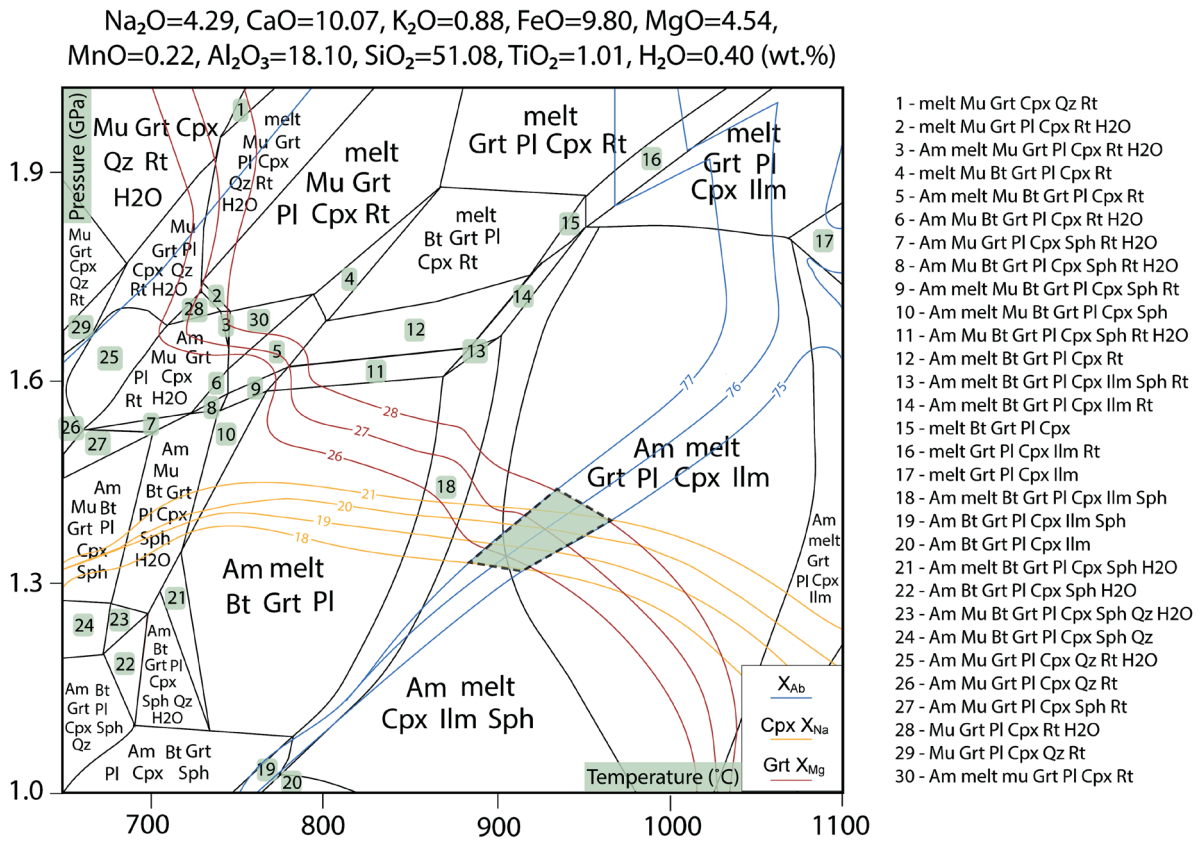

Fig. 4. P–T pseudosection of the granulite calculated in the NCKFMMnASHT system at conditions of T=650–1100 °C and P=1–2 GPa. Green field outlines the inetersection of compositional isopleths of X_{Ab}, X_{Na} in clinopyroxene and X_{Mg} in garnet. Mineral abbreviations: Am — amphibole, Bt — biotite, Cpx — clinopyroxene, Grt — garnet, Ilm — ilmenite, Mu — muscovite, Pl — plagioclase, Qz — quartz, Rt — rutile, Sph — sphene.

The thermodynamic phase equilibrium modelling suggests the HT equilibration conditions in the stability field of melt+plagioclase+garnet+clinopyroxene+amphibole+ilmenite (Fig. 4), thus indicating a favorable scenario for the stabilization of retrograde plagioclase in the observed assemblage. It is envisioned that the plagioclase intergrown with clinopyroxene should have formed earlier during decompression due to the breakdown of omphacite. Hence, the large plagioclase grains in the matrix that show textural equilibrium with the surrounding phases are considered to represent the part of the equilibrium assemblage. It is inferred here that it could have formed as a result of partial melt crystallization upon cooling. However, not much partial melt has been observed in the outcrop, hand specimens and even thin sections. Only rare multi-phase inclusions in garnet containing K-feldspar, plagioclase, pure albite and biotite may be indicative for partial melting and thus could confirm melt presence during the rock evolution (e.g., Ferrero et al. 2015). Alternatively, they might have resulted from a breakdown of an unidentified prograde Na-, Ca- and K-bearing hydrous mineral (white mica plus zoisite?), but the preserved remnants of white mica do not contain increased amount of Na nor Ca. However, the modelled pseudosection does predict partial melting. Hence, it is considered that the partial melting must have affected the studied rock to some degree, likely during the earliest stages of decompression from peak pressure conditions. The other metamorphic changes that occurred during decompression are expressed by the formation of diopside–plagioclase poikiloblasts at the expense of clinopyroxene with a more omphacitic compositions, by the replacement of phengite by biotite, and by growth of the matrix plagioclase, amphibole and biotite, as well as replacement of relict rutile by titanite. Especially the latter phenomenon is interpreted to have occurred at final stages of the metamorphic cycle under amphibolite facies conditions. Also, the sharp change of the composition of garnet in the outermost rim can be explained by retrogressive diffusion and exchange between garnet in mutual contact with clinopyrexene, amphibole and biotite (Fig. 3D) during decompression to granulite and farther decompression and cooling to amphibolite facies conditions.

The obtained P–T conditions for decompressional HT equilibration of the Midsund granulite are in line with those recently calculated for comparable HP granulites occurring just north-east of the study area, as presented by Engvik et al. (2018). These authors estimated minimum P–T conditions for HP granulites at 1.4–1.8 GPa and 900–1100 °C. It also supports the observations made by Ganzhorn et al. (2014), who reported pervasive partial melting and HT equilibration of

felsic gneisses in the study region. Hence, the results obtained in this study are in agreement with the general, regional trend of a temperature gradient increase towards this part of the WGR as suggested e.g. by Cuthbert et al. (2000). As noted by Engvik et al. (2018), the WGR was traditionally thought to be a relatively cold UHP terrane. Their results, coupled with these presented herein and other observations of granulitized eclogites from Nordøyane (e.g., Larsen et al. 1998; Butler et al. 2013) and farther northeast from northernmost Vestranden in the Roan area (Möller 1988), show that this part of the WGR must have undergone regional scale HT re-equilibration of the eclogitized orogenic root during the terminal stages of the Scandian collision. This, in turn, broadens our understanding of the Caledonian orogenic cycle and shows that the Scandinavian Caledonides may share more similarities with other hot orogens, such as the Bohemian Massif (but see also e.g., O'Brien & Rötzler 2003; Medaris et al. 2018), than previously envisioned. It also shows a clear need for further petrological exploration of the garnet–clinopyroxene–plagioclase rocks that are within both the Parautochthon and allochthons of the Scandinavian Caledonides in order to deliver comprehensive data on the evolution of this mountain belt.

Acknowledgements: Simon Cuthbert and Dirk Spengler are thanked for their constructive reviews. Chris Barnes is acknowledged for help with linguistic correction, and Marian Janák as well as Milan Kohút for editorial works. This research was supported by the National Science Centre (Poland) funded research project CALSUB no. 2014/14/ST10/00321.

References

Andersen T.B., Jamtveit B., Dewey J.F. & Swensson E. 1991: Subduction and eduction of continental crust: major mechanisms during continent–continent collision and orogenic collapse, a model based on the south Norwegian Caledonides. *Terra Nova* 3, 303–310.

Andersen T.B., Berry H.N., Lux D.R. & Andresen A. 1998: The tectonic significance of pre-Scandian $^{40}Ar/^{39}Ar$ phengite cooling ages in the Caledonides of western Norway. *J. Geol. Soc.* 155, 297–309.

Austrheim H., Corfu F., Bryhni I. & Andersen T.B. 2003: The Proterozoic Hustad igneous complex: a low strain enclave with a key to the history of the Western Gneiss Region of Norway. *Precambrian Res.* 120, 149–175.

Braathen A., Nordgulen Ø., Osmundsen P.-T., Andersen T.B., Solli A. & Roberts D. 2000: Devonian, orogen-parallel, opposed extension in the Central Norwegian Caledonides. *Geology* 28, 615–618.

Brueckner H.K. 1972: Interpretation of Rb–Sr ages from the Precambrian and Paleozoic rocks of southern Norway. *Am. J. Sci.* 272, 334–358.

Brueckner H.K., Carswell D.A. & Griffin W.L. 2002: Paleozoic diamonds within a Precambrian peridotite lens in UHP gneisses of the Norwegian Caledonides. *Earth Planet. Sci. Lett.* 203, 805–816.

Butler J.P., Jamieson R.A., Steenkamp H.M. & Robinson P. 2013: Discovery of coesite-eclogite from Nordøyane UHP domain, Western Gneiss Region, Norway: Field relations, metamorphic history, and tectonic significance. *J. Metamorph. Geol.* 31, 147–163.

Butler J.P., Jamieson R.A., Dunning G.R., Pecha M.E., Robinson P. & Steenkamp H.M. 2018: Timing of metamorphism and exhumation in the Nordøyane ultra-high-pressure domain, Western Gneiss Region, Norway: New constraints from complementary CA-ID-TIMS and LA-MC-ICP-MS geochronology. *Lithos* 310–311, 153–170.

Carswell D.A. & Harvey M.A. 1985: The intrusive history and tectonometamorphic evolution of the Basal Gneiss Complex in the Moldefjord area, west Norway. In: Gee D.G. & Sturt B.A. (Eds.): The Caledonide Orogen — Scandinavia and Related Areas. *Wiley*, Chichester, 843–858.

Carswell D.A., van Roermund H.L.M. & Wiggers de Vries D.F. 2006: Scandian Ultrahigh-Pressure Metamorphism of Proterozoic Basement Rocks on Fjørtoft and Otrøy, Western Gneiss Region, Norway. *Int. Geol. Rev.* 48, 957–977.

Castro A.E. & Spear F.S. 2017: Reaction overstepping and re-evaluation of peak P–T conditions of the blueschist unit Sifnos, Greece: implications for the Cyclades subduction zone. *Int. Geol. Rev.* 59, 548–562.

Connolly J.A.D. 1990: Multivariable phase diagrams: an algorithm based on generalized thermodynamics. *Am. J. Sci.* 290, 666–718.

Connolly J.A.D. 2005: Computation of phase-equilibria by linear programming: a tool for geodynamic modeling and its application to subduction zone decarbonation. *Earth Planet. Sc. Lett.* 236, 524-541.

Corfu F., Torsvik T.H., Andersen T.B., Ashwal L.D., Ramsay D.M. & Roberts R.J., 2006: Early Silurian mafic–ultramafic and granitic plutonism in contemporaneous flysch, Magerøy, northern Norway: U–Pb ages and regional significance. *J. Geol. Soc.* 163, 291–301.

Corfu F., Austrheim H. & Ganzhorn A.C. 2014: Localized granulite and eclogite facies metamorphism at Flatraket and Krakeneset, Western Gneiss Region: U–Pb data and tectonic implications. In: Corfu F., Gasser D. & Chew D.M. (Eds.): New Perspectives on the Caledonides of Scandinavia and Related Areas. *The Geological Society*, London, 425–442.

Cuthbert S.J., Carswell D.A., Krogh-Ravna E.J. & Wain A. 2000: Eclogites & eclogites in the Western Gneiss Region, Norwegian Caledonides. *Lithos* 52, 165–195.

DesOrmeau J.W., Gordon S.M., Kylander-Clark A.R.C., Hacker B.R., Bowring S.A., Schoene B. & Samperton K.M. 2015: Insights into (U)HP metamorphism of the Western Gneiss Region, Norway: A high-spatial resolution and high-precision zircon study. *Chem. Geol.* 414, 138–155.

Engvik A.K., Willemoes-Wissing B. & Lutro O. 2018: High-temperature, decompressional equilibration of the eclogite facies orogenic root (Western Gneiss Region, Norway). *J. Metamorph. Geol.* 36, 5, 529–545.

Ferrero S., Wunder B., Walczak K., O'Brien P.J. & Ziemann M.A. 2015: Preserved near ultrahigh-pressure melt from continental crust subducted to mantle depths. *Geology* 43, 5, 447–450.

Fossen H. 2010: Extensional tectonics in the North Atlantic Caledonides: a regional view. In: Law R.D., Butler R.W.H., Holdsworth R.E., Krabbendam M. & Strachan R.A. (Eds.): Continental Tectonics and Mountain Building: The Legacy of Peach and Horne. *Geol. Soc. S.P.* 335, 767–793.

Ganzhorn A.C., Labrousse L., Prouteau G., Leroy C., Vrijmoed J.C., Andersen T.B. & Arberet L. 2014: Structural, petrological and chemical analysis of syn-kinematic migmatites: Insights from the Western Gneiss Region, Norway. *J. Metamorph. Geol.* 32, 647–673.

Gee D.G. 1975: A tectonic model for the central part of the Scandinavian Caledonides. *Am. J. Sci.* 275A, 468–515.

Gee D.G. 1980: Basement-cover relationships in the central Scandinavian Caledonides. *GFF* 102, 455–474.

Gee D.G., Fossen H., Henriksen N. & Higgins A.K. 2008: From the eraly Paleozoic platforms of Baltica and Laurentia to the Caledonide orogen of Scandinavia and Greenland. *Episodes* 31, 44–51.

Gee D.G., Juhlin C., Pascal C. & Robinson P. 2010: Collisional Orogeny in the Scandinavian Caledonides (COSC). *GFF* 132, 29–44.

Gee D.G., Janák M., Majka J., Robinson P. & van Roermund H.L.M. 2013: Subduction along and within the Baltoscandian margin during closure of the Iapetus Ocean and Baltica–Laurentia collision. *Lithosphere* 5, 169–178.

Gilotti J.A. 2013: The Realm of Ultrahigh-Pressure Metamorphism. *Elements* 9, 255–260.

Glodny J., Kühn, A.K. & Austrheim H. 2008: Diffusion versus recrystallization processes in Rb–Sr geochronology: isotopic relics in eclogite facies rocks, Western Gneiss Region, Norway. *Geochim. Cosmochim. Acta* 72, 506–525.

Gordon S.M., Whitney D.L., Teyssier C., Fossen H., Kylander-Clark A. 2016: Geochronology and geochemistry of zircon from the northern Western Gneiss Region: Insights into the Caledonian tectonic history of western Norway. *Lithos* 246–247, 134–148.

Green E., Holland T. & Powell R. 2007: An order-disorder model for omphacitic pyroxenes in the system jadeite–diopside–hedenbergite–acmite, with applications to eclogitic rocks. *Am. Mineral.* 92, 1181–1189.

Green E.C.R., White R.W., Diener J.F.A., Powell R., Holland T.J.B. & Palin R.M. 2016: Activity-composition relations for the calculation of partial melting equilibria in metabasic rocks. *J. Metamorph. Geol.* 34, 9, 845–869.

Hacker B.R., Abers G.A. & Peacock S.M. 2003: Subduction factory. 1. Theoretical mineralogy, densities, seismic wavespeeds, and H2O contents. *J. Geophys. Res.* 108, B1, 2029.

Hacker B.R., Andersen T.B., Johnston S., Kylander-Clark A.R.C., Peterman E.M., Walsh E.O. & Young D. 2010: High-temperature deformation during continental-margin subduction and exhumation: the ultrahigh-pressure Western Gneiss Region of Norway. *Tectonophysics* 480, 1–4, 149–171.

Hacker B.R., Kylander-Clark A.R.C., Holder R., Andersen T.B., Peterman E.M., Walsh E.O. & Munnikhuis J.K. 2015: Monazite response to ultrahigh-pressure subduction from U–Pb dating of laser ablation split stream. *Chem. Geol.* 409, 28–41.

Harvey M.A. 1985: A geochemical and structural study of the gneisses and eclogites on the Molde Peninsula, West Norway. *Unpublished PhD thesis*, *University of Sheffield*, 1–272.

Holder R.M., Hacker B.R., Kylander-Clark A.R.C. & Cottle J.M. 2015: Monazite trace element and isotopic signatures of (ultra) high-pressure metamorphism: examples from the Western Gneiss Region, Norway. *Chem. Geol.* 409, 99–111.

Holland T.J.B. & Powell R. 2003: Activity-composition relations for phases in petrological calculations: an asymmetric multicomponent formulation. *Contrib. Mineral. Petrol.* 145, 4, 492–501.

Holland T.J.B. & Powell R. 2011: An improved and extended internally consistent thermodynamic dataset for phases of petrological interest, involving a new equation of state for solids. *J. Metamorph. Geol.* 29, 333–383.

Hollocher K., Robinson P., Terry M.P. & Walsh E. 2007: Application of major- and trace element geochemistry to refine U–Pb zircon, and Sm/Nd or Lu/Hf sampling targets for geochronology of HP and UHP eclogites, Western Gneiss Region, Norway. *Am. Mineral.* 92, 1919–1924.

Humphreys J.F. & Hatherley M. 1995: Recrystallization and related annealing phenomena. *Elsevier Science*, New York, 1–498.

Krill A.G. 1980: Tectonics of the Oppdal area, central Norway. *GFF* 102, 523–530.

Krogh T.E., Kamo S.L., Robinson P., Terry M.P. & Kwok K. 2011: U–Pb zircon geochronology of eclogites from the Scandian Orogen, northern Western Gneiss Region, Norway: 14–20 million years between eclogite crystallization and return to amphibolite-facies conditions. *Can. J. Earth Sci.* 48, 2, 441–472.

Kruhl J.H. 2001. Crystallographic control on the development of foam textures in quartz, plagioclase and analogue material. In: Dresen G. & Handy M. (Eds.): Deformation mechanisms, rheology and microstructures. *Int. J. Earth Sci*. 90, 104–117.

Kylander-Clark A.R.C., Hacker B.R., Johnson C.M., Beard B.L., Mahlen N.J. & Lapen T.J. 2007: Coupled Lu–Hf and Sm–Nd geochronology constrains prograde and exhumation histories of high- and ultrahigh-pressure eclogites from western Norway. *Chem. Geol.* 242, 137–154.

Kylander-Clark A.R.C., Hacker B.R. & Mattinson J.M. 2008: Slow exhumation of UHP terranes: titanite and rutile ages of the Western Gneiss Region, Norway. *Earth Planet. Sci. Lett.* 272, 3–4, 531–540.

Larsen R.B., Eide E.A. & Burke E.A.J. 1998: Evolution of microdiamond-bearing granulites in the Western Gneiss Region, Norway. *Contrib. Mineral. Petrol.* 133, 106–121.

Medaris G.L., Brueckner H.K., Cai Y., Griffin W.L. & Janák M. 2018: Eclogites in peridotite massifs in the Western Gneiss Region, Scandinavian Caledonides: Petrogenesis and comparison with those in the Variscan Moldanubian Zone. *Lithos* 322, 325–346.

Möller C. 1988: Geology and metamorphic evolution of the Roan area, Vestranden Western Gneiss Region, Central Norwegian Caledonides. *Norges Geol. Unders. Bull.* 413, 1–31.

O'Brien P.J. & Rötzler J. 2003: High-pressure granulites: formation, recovery of peak conditions and implications for tectonics. *J. Metamorph. Geol.* 21, 3–20.

Roberts D. 2003: The Scandinavian Caledonides: Event chronology, palaeogeographic settings and likely modern analogues. *Tectonophysics* 365, 283–299.

Roberts D. & Gee D.G. 1985: An introduction to the structure of the Scandinavian Caledonides. In: Gee D.G. & Sturt B.A. (Eds.): The Caledonide Orogen — Scandinavia and Related Areas. *Wiley,* Chichester, 55–68.

Robinson P. 1995: Extension of Trollheimen tectono-stratigraphic sequence in deep synclines near Molde and Brattvåg, Western Gneiss Region, southern Norway. *Norsk Geol. Tidsskr.* 75, 181–198.

Robinson P. & Hollocher K. 2008: Geology of Trollheimen. In: Robinson P., Roberts D. & Gee D.G. (Eds.): Guidebook: a tectonostratigraphic transect across the central Scandinavian Caledonides. *NGU report 2008.064, pt. II. NGU*, Trondheim, 61–67.

Root D.B., Hacker B.R., Gans P.B., Ducea M.N., Eide E.A. & Mosenfelder J.L. 2005: Discrete ultrahigh-pressure domains in the Western Gneiss Region, Norway: implications for formation and exhumation. *J. Metamorph. Geol.* 23, 45–61.

Røhr T.S., Corfu F., Austrheim H. & Andersen T.B. 2004: Sveconorwegian U–Pb zircon and monazite ages of granulite-facies rocks, Hisarøya, Gulen, Western Gneiss Region, Norway. *Norw. J. Geol.* 84, 251–256.

Røhr T.S., Bingen B., Robinson P. & Reddy S.M. 2013: Geochronology of Paleoproterozoic augen gneisses in the Western Gneiss Region, Norway: evidence for Sveconorwegian zircon neocrystallization and Caledonian zircon deformation. *J. Geol.* 121, 105–128.

Scambelluri M., Pettke T. & van Roermund H.L.M. 2008: Majoritic garnets monitor deep subduction fluid flow and mantle dynamics. *Geology* 36, 59–62.

Skår Ø. 2000: Field relations and geochemical evolution of the Gothian rocks in the Kvamsøy area, southern Western Gneiss Complex, Norway. *Norges Geol. Unders. Bull.* 437, 5–23.

Skår Ø. & Pedersen R.B. 2003: Relations between granitoid magmatism and migmatization: U–Pb geochronological evidence from the Western Gneiss Complex, Norway. *J. Geol. Soc. London* 160, 935–946.

Smith D.C. & Godard G. 2013: A Raman spectroscopic study of diamond and disordered sp^3-carbon in the coesite-bearing Straumen eclogite pod, Norway. *J. Metamorph. Geol.* 31, 19–33.

Spengler D. 2006: Origin and evolution of deep upper mantle rocks from western Norway. *Geologica Ultraiectina, Utrecht University* 266, 1–266.

Spengler D., Brueckner H.K., van Roermund H.L.M., Drury M.R. & Mason P.R.D. 2009: Long-lived, cold burial of Baltica to 200 km depth. *Earth Planet. Sci. Lett.* 281, 1–2, 27–35.

Terry M.P. & Robinson P. 2004: Geometry of eclogite-facies structural features: Implications for production and exhumation of ultrahigh-pressure and high-pressure rocks, Western Gneiss Region, Norway. *Tectonics* 23, TC2001.

Terry M.P., Robinson P., Hamilton M.A. & Jercinovic M.J. 2000: Monazite geochronology of UHP and HP metamorphism, deformation and exhumation, Nordøyane, Western Gneiss Region, Norway. *Am. Mineral.* 85, 1651–1664.

Tucker R.D. 1986: Geology of the Hemnefjord–Orkanger area, south central Norway. *Norges Geol. Unders. Bull.* 404, 1–20.

Tucker R.D., Krogh T.E. & Råheim A. 1990: Proterozoic evolution and age–province boundaries in the central Western Gneiss Region, Norway: results of U–Pb dating of accessory minerals from Trondheimsfjord to Geiranger. In: Gower C.F., Rivers T. & Ryan B. (Eds.): Mid-Proterozoic Laurentia–Baltica. *Geological Association of Canada, Special Paper* 38, 149–173.

Tucker R.D., Robinson P., Solli A., Gee D.G., Thorsnes T., Krogh T.E., Nordgulen Ø. & Bickford M.E. 2004: Thrusting and extension in the Scandian hinterland, Norway: New U–Pb ages and tectonostratigraphic evidence. *Am. J. Sci.* 304, 6, 477–532.

van Roermund H.L.M. 2009a: Recent progress in Scandian ultra-high-pressure metamorphism in the northernmost domain of the Western Gneiss Complex, SW Norway: Continental subduction down to 180-200 km depth. *J. Geol. Soc. London* 166, 4, 739–751.

van Roermund H.L.M. 2009b: Mantle-wedge garnet peridotites from the northernmost ultra-high pressure domain of the Western Gneiss Region, SW Norway. *Eur. J. Mineral.* 21, 6, 1085–1096.

van Roermund H.L.M. & Drury M.R. 1998: Ultra-high pressure (P>6 GPa) garnet peridotites in Western Norway: exhumation of mantle rocks from >185 km depth. *Terra Nova* 10, 295–301.

van Roermund H.L.M., Spengler D. & Wiggers de Vries-Dekkers D. 2005: Evidence for ultra-high pressure (UHP) metamorphism within Proterozoic basement rocks on Otrøy, Western Gneiss Region, Norway. *Mitteilungen der ÖMG* 150, 159.

Vrijmoed J.C., van Roermund H.L.M. & Davies G. 2006: Evidence for diamond-grade UHP metamorphism and fluid interaction in the Svartberget Fe–Ti garnet peridotite/websterite body, Western Gneiss Region, Norway. *Mineral. Petrol.* 88, 381–405.

Vrijmoed J.C., Smith D.C. & van Roermund H.L.M. 2008: Raman confirmation of microdiamond in the Svartberget Fe–Ti type garnet peridotite, Western Gneiss Region, Western Norway. *Terra Nova* 20, 295–301.

Walsh E.O., Hacker B.R., Gans P.B., Grove M. & Gehrels G. 2007: Protolith ages and exhumation histories of (ultra) high-pressure rocks across the Western Gneiss Region, Norway. *Geol. Soc. Am. Bull.* 119, 289–301.

White R.W., Powell R. & Holland T.J.B. 2007: Progress relating to calculation of partial melting equilibria for metapelites. *J. Metamorph. Geol.* 25, 511–527.

White R.W., Powell R., Holland T.J., Johnson T.E. & Green E.C. 2014: New mineral activity–composition relations for thermodynamic calculations in metapelitic systems. *J. Metamorph. Geol.* 32, 261–286.

Young D.J., Hacker B.R., Andersen T.B. & Corfu F. 2007: Amphibolite to ultrahigh-pressure transition in western Norway: implications for exhumation tectonics. *Tectonics* 26, TC1007, 1–15.

Young D.J. 2017: Structure of the (ultra)high-pressure Western Gneiss Region, Norway: Imbrication during Caledonian continental margin subduction. *Geol. Soc. Am. Bull.* 130, 5–6, 926–940.

Young D.J. & Kylander-Clark A.R.C. 2015: Does Continental Crust Transform during Eclogite-Facies Metamorphism? *J. Metamorph. Geol.* 33, 331–357.